J Mater Sci (2013) 48:7088–7096
DOI 10.1007/s10853-013-7521-4

Preparation and characterization of micro and nanocomposites based on poly(vinyl alcohol) for packaging applications

Romina P. Ollier · Claudio J. Perez · Vera A. Alvarez

Received: 19 April 2013 / Accepted: 8 June 2013 / Published online: 19 June 2013

Abstract In the present work, micro and nano composites based on poly(vinyl alcohol) matrix reinforced with cellulose (micro) and bentonite (nano) were obtained by film casting. The resulting composite materials were characterized by means of differential scanning calorimetry, thermogravimetric analysis, X-ray diffraction, FTIR spectroscopy, water absorption, permeability, and mechanical tests. The effect of the micro and nano fillers on the thermal, mechanical, and water absorption properties of the matrix was determined. The effects of polymer molecular weight and processing steps were also studied. Based on the results of the work, the potential biodegradability and the low cost of the starting materials, it can be concluded that the produced materials may be promising for packaging applications.

Introduction

In the last decades, poly(vinyl alcohol) (PVOH) has received great attention due to its unique physical and chemical properties [1, 2]. PVOH is a well-known non-toxic, water-soluble, and biocompatible synthetic polymer. As it is a polyhydroxy polymer, PVOH is characterized by a strong hydrophilic and hydrogen bonding character [3, 4]. It has an excellent film-forming ability; thermal stability; chemical resistance, good transparency, and flexibility, and because of them, it is widely used in several applications such as paper coating, packing, biomedical devices, and membrane preparation [5, 6]. The properties of the PVOH are affected by the molecular weight and the degree of hydrolysis [7, 8], because it is obtained by the hydrolysis of poly(vinyl acetate). Depending on the degree of hydrolysis, different types of PVOH can be produced, leading to different amounts of hydroxyl groups in the polymer. Although there are several works related to this polymer, there are no systematic studies of the effect of the molecular weight on the mechanical properties and water absorption of PVOH films. However, some applications are still restricted because of its high degree of swelling and solubility in water, as well as its limited mechanical properties [9]. Some of these properties can be enhanced by the incorporation of reinforcement. Concerning packaging applications, several parameters, including the moisture content, the degree of crystallinity, and the presence of additives or reinforcements, affect the mass transport properties of the polymers. In addition to the barrier properties, the thermal and the mechanical properties of the final material are of great importance for both the processing and efficient use of these materials. The preparation of a composite material that incorporates both biocompatibility and improved physical properties, by use of natural fillers, is of great importance for packaging and in food industry [10].

The use of microcellulose (MC), which is a natural polysaccharide with excellent mechanical properties and high aspect ratio, as reinforcement is attractive due to environmental and economic concerns [11]. Improvements on thermal stability, tensile strength, and water resistance

R. P. Ollier · V. A. Alvarez (✉)
Composite Materials Group (CoMP), Research Institute of Material Science and Technology (INTEMA), CONICET—National University of Mar del Plata (UNMdP), Solís 7575, 7600 Mar del Plata, Argentina
e-mail: alvarezvera@fi.mdp.edu.ar

C. J. Perez
Polymer Science and Technology Group, Research Institute of Material Science and Technology (INTEMA), CONICET—National University of Mar del Plata (UNMdP), Av. J.B. Justo 4302, 7600 Mar del Plata, Argentina

by different whiskers incorporation were reported but the literature is still limited and incomplete [12–14].

Clay minerals, which are a diverse class of layered silicates, are also popular fillers for various polymeric materials. Their crystalline net consists of bi-dimensional layers where a central octahedral layer of either alumina or magnesia is joined to two external tetrahedrons of silica in such a way that the oxygen ions of the octahedral layer also belong to the tetrahedral layers [15, 16]. Among these reinforcements, the use of bentonite (montmorillonite-based layered silicate clay) is interesting because added to their environmental and economic importance, their natural abundance, swelling properties, and their mechanical and chemical resistance makes them very useful as polymeric reinforcements [17]. Dispersing clays in polymers at the nanoscale, even at loadings of only 1–5 wt%, provides considerable improvements in polymer properties compared with conventional micro particle fillers including, for example, higher modulus both in solid and melt state, increased strength and thermal stability, decreased permeability, and increased biodegradability [15, 18]. The main reason for these enhanced properties in nanocomposites is the stronger interfacial interaction between the matrix and layered silicate, compared with conventional filler-reinforced systems. In order to achieve these better properties it is necessary to obtain a totally exfoliated structure (this means that the silicate layers are completely and uniformly dispersed in the continuous polymeric matrix).

As most of the polymers are hydrophobic, it is necessary to make a previous treatment to the polymer or the filler so as to make them more compatible. Usually, the hydrophilic silicates are transformed to organophilic ones by means of cation exchange reactions. In fact, in previous works we have analyzed the effect of a commercial organo-modified montmorillonite (Cloisite 30B) [19] and a laboratory organo-modified bentonite [20] on the morphology and mechanical properties of polycaprolactone (PCL)/clay nanocomposites prepared by melt intercalation and casting for packaging applications. Besides, Casco et al. [21] carried out several treatments: alkaline-treatments; acetylation, and esterification with stearic and lauric acids on cellulose fibers previous to mixing them with PCL matrix. Despite the fact that these chemical treatments may be simple, they are time consuming because of the additional steps, they make the preparation procedure more complicated, and they also elevate the final cost of the composite material. All these factors are extremely important, especially in industrial applications. However, PVOH/bentonite and PVOH/microcellulose composites can be easily prepared because, as all of them are very hydrophilic, they can be incorporated into the PVOH without any need for pretreatment by simply dispersing the two components in distilled water, which is another remarkable point. In addition, a highly hydrolyzed PVOH is used in order to have a good compatibility with the fillers [6]. Thus, a composite material of PVOH and cellulose or clay with improved mechanical properties is likely to obtain in a cost-effective way [22].

The aim of this work was, first, to analyze the effect of the molecular weight of the polymer on the final properties of the materials and to select the most adequate of them for the subsequent composites; then, to obtain PVOH/cellulose microcomposites and PVOH/clay nanocomposites and to analyze the effect of the filler on the behavior of the neat matrix. In the case of nanocomposites, only a low silicate loading was studied (5 wt%), which is relevant for a potential application. Different processing steps were studied because in this kind of materials the final properties depend on the type of produced composite (i.e., microcomposite, intercalated nanocomposite, or exfoliated nanocomposite) and the developed morphology is also dependent on the processing variables. In the case on microcomposites, MC loadings between 5 and 20 wt% were used. The composites exhibited high levels of filler dispersion inside the polymer matrix, due to favorable interactions. The obtained materials were characterized by X-ray diffraction (XRD), scanning electron microscopy (SEM), UV–Visible spectroscopy, FTIR spectroscopy, differential scanning calorimetry (DSC), thermogravimetric analysis (TGA), mechanical and impact tests, water vapor transmission, and water absorption studies. The research work was carried out to evaluate the potential use of these novel composite materials as packaging films.

Experimental

Materials

PVOH of different molecular weight M_w (PVOH1: 31000–50000 g/mol; PVOH2: 89000–98000 g/mol; PVOH3: 124000–186000 g/mol) with a degree of hydrolysis higher than 98 % were purchased from Sigma-Aldrich.

Microcrystalline cellulose powder from Sigma-Aldrich was used as received to prepare the microcomposites.

Bentonite, supplied by Minarmco S.A. (Neuquén, Argentina), was used as received to prepare the nanocomposites.

Preparation of the films

PVOH and PVOH/MC, PVOH/bentonite films were prepared by casting technique, adapted from Sharaf et al. [23]. PVOH solution was prepared by dissolving 2 g of PVOH in distilled water (98 ml) and maintained for 24 h at room temperature to allow the swelling process. Then, the solution was heated to 90 °C and stirred using a magnetic

stirrer for 4 h to ensure the complete dissolution of the polymer. The solution was then poured into glass plate dishes and it was dried in an oven during 48 h at 40 °C. Homogeneous films of 0.1–0.2 mm of thickness were obtained.

In order to analyze *the effect of molecular weight*, the PVOH with different molecular weights previously mentioned were used following the described procedure. The material with the most adequate properties for packaging applications was chosen as the matrix for the subsequent composites.

In the case of *microcomposites*, three different amounts of cellulose were used: 5, 10, and 20 wt%. The cellulose microfibers were previously placed in distilled water (proportion: 1 g cellulose/100 ml distilled water) and the suspension was incorporated before stirring the PVOH solutions; the rest of the procedure was the same.

In the case of *nanocomposites*, 5 wt% of bentonite was employed. In this case, different incorporation steps were studied: (i) PVOH + Clay (swelling 24 h in water at room temperature in separated flasks), named NA; (ii) PVOH (24 h in water at room temperature) + Clay (dried), named NB; (iii) PVOH + Clay (swelling together 24 h in water at room temperature), named NC.

Methods

Thermogravimetric Analysis (TGA) measurements were carried out by using a Shimadzu TGA-50 thermal analyzer. The samples were heated from 25 to 1000 °C at a heating rate of 10 °C/min under constant nitrogen flow.

Differential Scanning Calorimetry (DSC) tests were performed in a DSC Perkin Elmer 7 differential scanning calorimeter from 25 to 250 °C at a heating rate of 10 °C/min under nitrogen atmosphere (ASTM D3417) in aluminum pans. The glass transition temperature (T_g) and melting temperature (T_m) of the samples were obtained from the curves. The degree of crystallinity (X_{cr}) was calculated from the following equation:

$$X_{cr}(\%) = \frac{\Delta H_f}{w_{PVOH} \times \Delta H_{100}} \times 100 \quad (1)$$

where ΔH_f is the experimental heat of fusion obtained from the area of the melting peak, w_{PVOH} is the PVOH weight fraction, and ΔH_{100} is the heat of fusion of 100 % crystalline PVOH and its value is 150 J/g [24].

X-Ray Diffraction (XRD) patterns of bentonite and nanocomposites were obtained from a PW1710 diffractometer equipped with a monochromatic CuKα radiation source ($\lambda = 1.5406$ Å) operating at 45 kV, 30 mA, at a scanning rate of 2°/min, and a step size of 0.02°.

Tensile tests were performed in a universal testing machine Instron 4467 at a constant crosshead speed of 2 mm/min and a load cell of 100 N. The test specimens were prepared according to the ASTM D882 by cutting films into dog-bone shapes using a template. The sample length was 63 mm, the width was 16 mm, and the distance between clamps was 28 mm. Before tests, all the samples were dried under vacuum until constant weight. Tests were carried out at room temperature. All measurements were done in at least four replicates, and the values were averaged.

Impact tests (Puncture tests) were conducted on 30-mm-diameter samples cut out from a molded film. These tests were performed in a falling weight Fractovis of Ceast at 1 m/s. From these tests, load–displacement curves were obtained. The total energy required to penetrate the specimen completely, E_{tot}, is the total area under the load–displacement curve also normalized by the sample thickness. All measurements were done in at least four replicates, and the values were averaged.

Scanning electron microscopy (SEM, model JEOL JSM 6460 LV) was used to observe the morphology of microcellulose fibers and PVOH/MC microcomposites after they had been coated with a thin layer of gold, at an accelerating voltage of 10 kV. All microcomposites were previously fractured in liquid nitrogen in a direction perpendicular to the stretch direction.

Infrared Spectroscopy (FTIR) spectra were obtained on a Perkin–Elmer Spectrophotometer model Spectrum 100 in attenuated total reflection (ATR) mode. Spectra, averaged over 16 scans, were taken in the range of 4000–600 cm^{-1} at a resolution of 4 cm^{-1}. It is important to note that the spectra of both sides of all the films displayed the same number of peaks and the positions and relative intensities of these peaks were identical.

Ultraviolet–Visible (UV–Vis) spectra of the polymer films were recorded on an Agilent 8453 photodiode array spectrophotometer. The samples were prepared by cutting pieces of the cast films.

Water absorption tests were carried out in an environment at room temperature, with controlled relative humidity (RH), simulated from a solution of water and glycerin. Before tests, all the samples were dried under vacuum until constant weight. All conditioned samples were weighed at prefixed times and the moisture absorption values at each time were calculated using the following equation:

$$M_t(\%) = \frac{M_t - M_0}{M_0} \times 100 \quad (2)$$

where M_t is the mass of the sample at a time t and M_0 is the initial mass of the sample (dried).

Water vapor transmission rates (WVTR) were studied following a gravimetric technique from Razzak et al. [25]. Samples with a diameter of 28 mm (without physical

defects such as cracks or bubbles) and a thickness of about 0.1 mm were cut and then put as a cap at the mouth of a bottle with a diameter of about 25 mm containing 20 ml of deionized water. Once, the films were secured, each bottle was placed in a chamber for 10 days at constant temperature of 22 °C and 65 % RH. All samples, prior to their testing, were conditioned for 3 days at the same relative humidity. The WVTR of each sample was calculated using the following equation:

$$\mathrm{WVTR}\left(\frac{\mathrm{g}}{\mathrm{h}\times \mathrm{m}^2}\right) = \frac{W_\mathrm{i} - W_\mathrm{f}}{240 \times A} \times 10^6 \quad (3)$$

where A is the area of bottle mouth (mm^2), W_i and W_f are the weight of the system (bottle and film cap) before and after placing in the chamber, respectively. The permeability values presented in the manuscript were the average values of three permeation experiments.

Results and discussion

Effect of molecular weight on the behavior of PVOH films

Table 1 summarizes the results of thermal and mechanical characterization for PVOH as a function of molecular weight. First of all, it can be noticed that an increase in the molecular weight produced a clear decrease on the elastic modulus and a reduced tensile strength which could be directly related with a reduced crystalline phase (the values of this parameter are shown in Table 1) which has better mechanical properties than the amorphous phase. The increment on the molecular weight produces an increase on the chain disorder, increasing the amorphous content and so, reducing the mechanical properties. Pure PVOH is partially crystalline and consists of crystalline layers or lamellas of folded chains joined together by tie molecules, which form amorphous regions between the lamellas [26]. Thus, an increase of molecular weight will lead to a higher degree of disorder.

The effect of polymer molecular weight on the impact behavior of PVOH is also displayed on Table 1. It is clear that the increase of the polymer molecular weight produced enlarged impact properties, which is in accordance with the decrease on the tensile strength [27].

Based on the obtained results, PVOH2 was selected to prepare the micro and nanocomposites and to analyze the effect of the fillers in the general behavior of the matrix because it exhibits a good balance between the mechanical and impact properties, and an intermediate value of crystallinity degree.

Effect of filler incorporation on the behavior of PVOH films

Microcomposites

The MC fibers have a crystallinity index of 65 %, obtained from XRD (from this study, it was also determined that they were Cellulose I). The maximum temperature of degradation (obtained from TGA) was around 363 °C; they absorb 6.3 % of moisture in 24 h at 90 % RH. From Fig. 1a it was determined that the average length and diameter of the microfibers were: 144.3 ± 18.6 and 65.5 ± 37.0 μm, respectively.

Regarding PVOH/MC films, although all the produced films were transparent, which is important for packaging, for high cellulose content this transparency was reduced. From the observation of Table 2, it can be observed that for lower contents of MC (5 and 10 wt%) the differences in the crystallinity of microcomposites are included between the dispersion of the measurements, so no important variations were detected. The slight increase of crystallinity for 20 wt% MC composite is possibly related to the nucleating effect of cellulose fibers, which was previously observed in literature for PVOH/MC films [28]. On the other hand, it is clear that the glass transition temperature (Matrix: 102.5 °C) increased not only with the incorporation of MC but also as a function of cellulose content, which could be related with the PVOH–MC interactions which restrict the capability of the matrix to move [29]. Regardless the composition, there are no important changes on the melting temperature with the incorporation of cellulose microfibers; a similar trend was observed in literature [28].

Table 2 also presents the values of water uptake once equilibrium is reached at long times (M_∞), which is the maximum water absorption that each material can incorporate. It is known that moisture affects the integrity of plastic packaging. Besides, one of the major drawbacks in

Table 1 Characteristics of PVOH films as a function of the molecular weight

Sample	M_w (g/mol)	X_cr (%)	T_g (°C)	T_m (°C)	E (MPa)	σ (MPa)	E_impact (J/mm)
PVOH1	31000–50000	39.4	110.4	190.8	85 ± 8	21 ± 1	1.7 ± 0.2
PVOH2	89000–98000	35.8	102.5	228.3	68 ± 7	17 ± 1	3.6 ± 0.2
PVOH3	124000–186000	27.1	99.0	223.4	49 ± 6	16 ± 1	4.3 ± 0.3

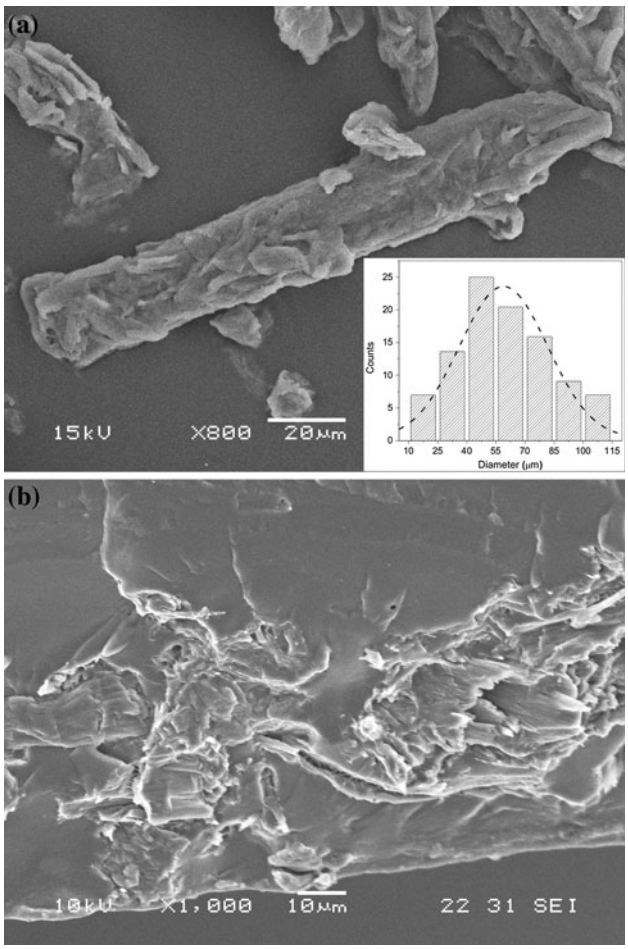

Fig. 1 SEM micrographs of **a** MC fiber with diameter distribution curve of MC fibers (*inset*); **b** cross-section of PVOH/10 wt% MC microcomposite

the use of PVOH-based materials is its water absorption tendency. Therefore, the knowledge of the moisture–water uptake of the materials and any improvement in water resistance is of great importance. The table shows that the microcomposites absorbed less water than the matrix; and it decreased with the increase of cellulose content. This result is related to the interactions between cellulose and PVOH through the hydroxyl groups, decreasing the possibility of water absorption with the increase of cellulose content.

Water vapor is one of the main permeants studied in packaging applications, because they may transfer from the internal or external environment through the polymer package wall, affecting the product quality and shelf-life [30]. The WVTR of neat PVOH and PVOH/MC microcomposites were calculated and the results are shown in Table 2. It can be observed that the presence of crystalline fibers along the polymer matrix is thought to increase the tortuosity of the permeation path leading to slower diffusion processes and, hence, to lower WVTR values [31]. No important changes were observed as a function of cellulose content.

The FTIR spectra of PVOH, MC, and PVOH/MC microcomposites are presented in Fig. 2a. The broad absorption band at 3700–3100 cm^{-1} in the FTIR spectra of MC corresponds to the –OH groups present in cellulose and at 2897 cm^{-1} due to CH stretching. The absorbance intensity at 1428 cm^{-1} is assigned as CH_2 bending; CH_2 wagging is localized at 1316 cm^{-1}; the peak at 1281 cm^{-1} is due to CH deformation; OH in-plane bending occurs at 1202 cm^{-1}; the peak at 1161 cm^{-1} is assigned to C–O–C asymmetric stretching; C–O stretching absorbs at 1030 cm^{-1}; and the peak 897 cm^{-1} is assigned as β-glucosidic linkage for the cellulose I [32]. The pure PVOH sample shows a broad band at 3100–3600 cm^{-1} due to the –OH stretching; the dual absorption peaks of symmetrical and asymmetrical stretching vibration of CH_2 appear at 2940–2904 cm^{-1}; and the peaks at 1418 and 1093 cm^{-1} are due to C–O group [33]. The addition of MC to PVOH has a slight effect on different regions of the FTIR spectra. Compared to the neat matrix, the peak of OH stretching vibration (situated at 3276 cm^{-1} for PVOH) shifted to 3284, 3288, and 3286 cm^{-1} for samples with 5, 10, and 20 wt%, respectively. The presence of MC in PVOH composites is also evidenced by the peak at about 1063 cm^{-1}, which is not present in the spectra of neat PVOH. Moreover, the peak at 1418 cm^{-1} for MC-free PVOH shifted to 1427, 1429, and 1426 cm^{-1} with the incorporation of 5, 10, and 20 wt% MC , respectively. All these changes can be explained in terms of the interactions between the host polymer chains and the reinforcement which alter the frequency of vibration of certain bonds.

The effect of microcellulose content on the mechanical properties, Young's modulus (E) and tensile strength (σ), of PVOH microcomposites is displayed on Fig. 3a, b, respectively. All properties were normalized by the measured bulk PVOH value (extracted from Table 1). It can be

Table 2 Water absorption after 20 days at 90 % RH, WVTR values and thermal characteristics of PVOH matrix and microcomposites

Cellulose content (wt%)	$M_{20\ days}$ at 90 % HR (%)	WVTR ($g/h/m^2$)	$T_{degradation}$ (°C)	X_{cr} (%)	ΔT_g^a (°C)
0	23.5 ± 2.0	14.0 ± 0.9	280	43.7 ± 2.0	–
5	18.5 ± 2.0	11.9 ± 0.9	288	42.2 ± 1.2	3.4
10	17.3 ± 1.9	12.9 ± 1.1	327	40.8 ± 2.2	16.0
20	16.4 ± 1.8	11.4 ± 0.5	346	44.3 ± 1.5	18.1

[a] $\Delta T_g = T_{g_{composite}} - T_{g_{matrix}}$

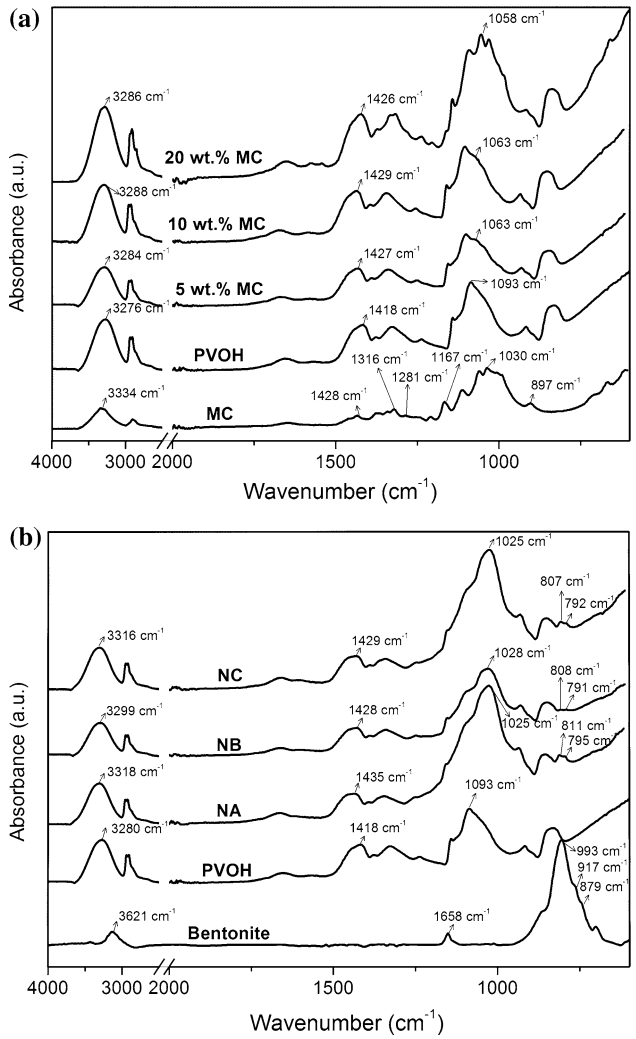

Fig. 2 FTIR spectra of **a** pure PVOH, MC, and microcomposites; **b** pure PVOH, bentonite, and nanocomposites

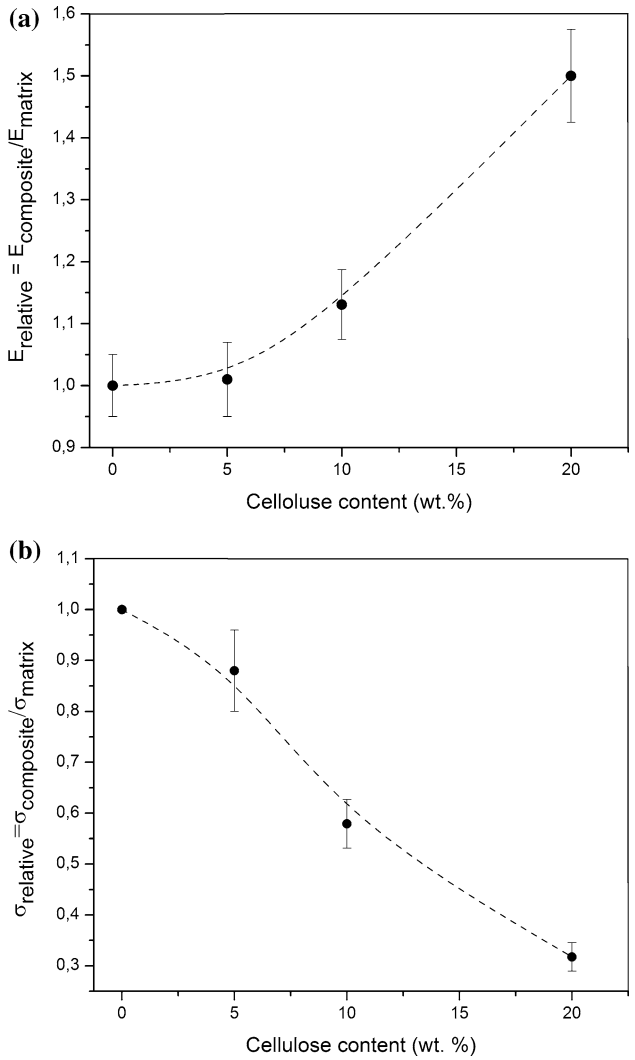

Fig. 3 Mechanical properties of PVOH/MC microcomposites relative to the matrix as a function of MC content **a** Young's modulus and **b** tensile strength

noticed that the Young's modulus increased as a function of cellulose content. One explanation for this effect could be related to the formation of a networked structure resulting from hydrogen bonding [34, 35]. To explain the increment on this property several factors have to be taken into account: the relative modulus of the filler compared with the matrix, since Young's modulus for MC is much higher that for PVOH; the hydrogen bonding between the PVOH chains and the cellulose microfibrils and so, the interfacial adhesion (Fig. 1b); the increase on the degree of crystallinity and finally the cellulose content. On the other hand, the tensile strength decreased as a function of cellulose content [29].

Nanocomposites

The cation exchange capacity of the natural bentonite, which was determined with $BaCl_2$ compulsive exchange method developed by Gillman and Sumpter [36], was 28.73 meq/100 g of clay. The interlaminar spacing was 1.28 nm and the absorbed moisture after 24 h at 90 % RH was 19.71 % [20].

By casting from an aqueous solution, the obtained PVOH matrix was a transparent and flexible film and the PVOH/bentonite nanocomposites still showed flexibility while maintaining the optical transparency of the matrix.

Figure 4 displays XRD curves of bentonite, PVOH, and PVOH/bentonite nanocomposites in the region from 2θ = 2–35°. The d_{001} values, corresponding to the (001) crystallographic plane in the crystal structure of the clay were calculated by using the Bragg's equation:

$$n \cdot \lambda = 2 \cdot d \cdot \sin\theta \quad (4)$$

where n = order of reflection (1), λ = wavelength of the source, θ = diffraction angle, and d = interplanar distance. The XRD curve for neat bentonite showed a peak angle at

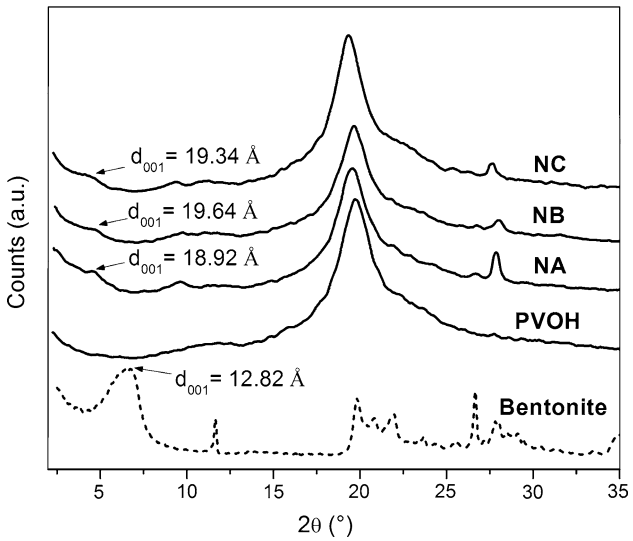

Fig. 4 XRD patterns of neat bentonite and PVOH/bentonite nanocomposites

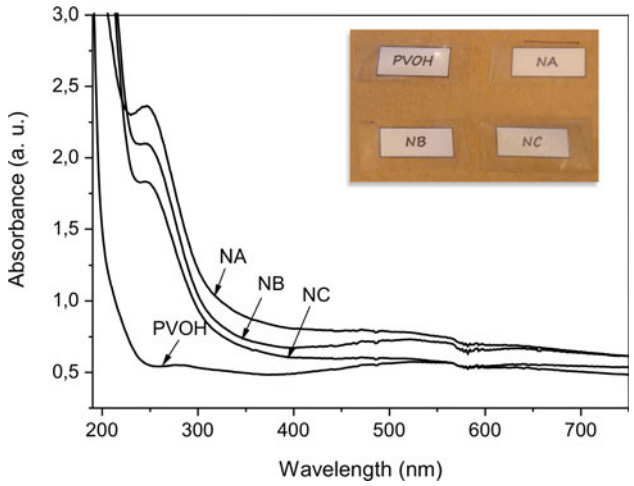

Fig. 5 UV–Visible spectra and visual observation (*inset*) of pure PVOH and PVOH/bentonite nanocomposites

$2\theta = 6.71°$ with a corresponding d-spacing of 1.28 nm. From the observation of Fig. 4 it is clear that all nanocomposites exhibited an intercalated–exfoliated structure due to the increase in the basal spacing of the clay [15]. This is because the hydroxyl groups of PVOH interact directly with the Na^+ cations and water molecules that are present between the clay platelets, as well as with the hydroxyl groups of the negatively charged layers of bentonite, leading to a high compatibility [37]. This enables the entrance of PVOH chains into the interlayer galleries, along with an increase in d-spacing between clay platelets. Another diffraction peak is observed at $2\theta = 19.5°$, corresponding to PVOH crystal reflections [38].

The FTIR spectra of PVOH, bentonite, and PVOH/bentonite nanocomposites are presented in Fig. 2b. The spectra of neat bentonite has an important peak at 3621 cm^{-1} corresponding to the structural OH groups of the clay whereas the peak at 1658 cm^{-1} corresponds to free water adsorbed by the clay (OH stretching). The strong absorption at 993 cm^{-1} is attributed to Si–O–Si in-plane vibrations [39]; the absorption peak of stretching vibration of Al–O–H appears at 917 cm^{-1}, whereas the peak at 879 cm^{-1} is due to Mg–O–H vibration [40]. The interactions between bentonite and PVOH in the nanocomposites are evidenced in different zones of FTIR spectra. In general terms, these changes are more evident for the NA and NC composites. The O–H stretches, which appear at 3280 cm^{-1} for neat PVOH, shifted to 3318, 3299, and 3316 cm^{-1} for NA, NB, and NC, respectively. Another shift is observed for the peak at 1418 cm^{-1}, which appears at 1435, 1428, and 1429 cm^{-1} for NA, NB, and NC. An additional indication of the presence of bentonite in PVOH is the observation of the peaks situated at about 1024, 807, and 792 cm^{-1} which are not present in the spectra of pure PVOH. The above analysis suggests that PVOH structure is altered by the interactions with the surface of bentonite platelets as a result of some additional peaks and shifts in frequencies of certain bonds when compared with pure PVOH.

One important issue is the increasing demand for transparency for certain applications where product visibility is required [41]. Figure 5 shows the UV/Visible characterization of pure PVOH and PVOH/bentonite nanocomposite films. Neat PVOH practically does not absorb above 250 nm, due to the very high hydrolysis degree of the polymer. Because of the nanoscale dispersion of the bentonite in the PVOH matrix, the nanocomposites samples retain the PVOH high optical clarity, in all cases. Indeed, the spectra show that the visible region, between 400 and 700 nm, is not affected by the presence of the clay and the high transparency of the PVOH is retained [42, 43], thus reflecting that there is no scattering due to the clay. These observations are in agreement with the results obtained from XRD patterns.

Table 3 presents the thermal characterization of PVOH nanocomposites. From TGA experiments it was observed that the first weight loss takes place between 55 and 160 °C due to the loss of adsorbed moisture; the major weight loss is at the second step between 200 and 500 °C, which corresponds to the structural decomposition of the PVOH [44, 45]. The change in thermal stability due to the incorporation of bentonite was not significant [46]. After 600 °C, the main products are mainly inorganic residues.

DSC experiments reveal a decrease in the degree of crystallinity of PVOH with the incorporation of the nano reinforcement in all cases. Furthermore, compared with the neat matrix, the T_g PVOH/bentonite nanocomposites shifted slightly toward higher values, indicating that bentonite platelets decrease the segmental motion of PVOH chains [47]. However, the neat PVOH has a melting temperature

Table 3 Water absorption after 20 days at 90 % RH, WVTR values and thermal characteristics of PVOH matrix and nanocomposites

Material	$M_{20\ days}$ at 90 % HR (%)	WVTR (g/h/m^2)	$T_{degradation}$ (°C)	X_{cr} (%)	ΔT_g^a (°C)
Matrix	26.8 ± 1.0	14.0 ± 0.9	280.4	52.7	–
NA	22.6 ± 1.0	11.2 ± 0.2	288.4	46.5	4.5
NB	21.8 ± 0.9	13.9 ± 0.9	279.8	41.4	6.1
NC	22.5 ± 0.6	12.5 ± 0.8	279.3	41.1	3.9

[a] $\Delta T_g = T_{g_{composite}} - T_{g_{matrix}}$

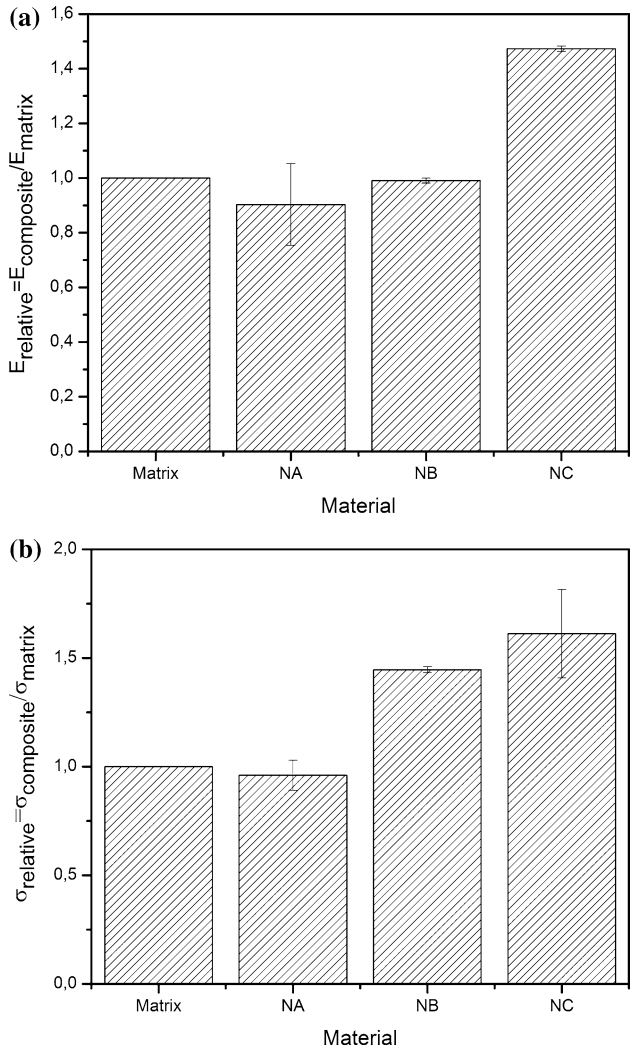

Fig. 6 Mechanical properties of PVOH/bentonite nanocomposites relative to the matrix: **a** Young's modulus and **b** tensile strength

of 229 °C and this parameter was practically not affected with the addition of bentonite.

Water absorption of nanocomposites after 20 days at 90 % RH is also shown in Table 3. An important fact is that the addition of clay reduces the absorption of moisture, which is one of the important drawbacks of PVOH as we have previously said. This could be related to the fact that the clay platelets dispersed in a nanometric scale significantly increase the tortuosity of the path for the permeation of water molecules through the polymeric matrix [43, 48]. It can also be noticed that WVTR was diminished by the incorporation of clay particles in the case of NA (20 % lower that neat PVOH) and NC (11 % lower than neat PVOH), whereas NB displayed no significant effect on the WVTR values in comparison to the matrix, possibly due to the worst dispersion of the clay nanoplatelets. Again, the reduced permeability of nanocomposites is mainly attributed to the increase in tortuosity caused by the impermeable platelets distributed in the polymer matrix as well as to the strong interfacial interaction [49].

Figure 6 shows the effect of the incorporation of bentonite on the mechanical properties of matrix and nanocomposites. For comparison, the all properties were normalized by the measured bulk PVOH value. It can be noticed that the modulus of NA and NB remained almost constant compared to the matrix, whereas the modulus of NC was improved probably due to the method of preparation of the composite. The same behavior is seen in the resistance of materials. So the best results were obtained for the compound NC. This can be attributed to better distribution of clay in the matrix.

Conclusions

In this work, it was found that the increase in the molecular weight of PVOH produced a decrease on the tensile mechanical properties which was attributed to the decrease on the degree of crystallinity associated with the higher disordered phase content. Based on these findings, an intermediate molecular weight of PVOH was selected to prepare the polymer composites.

Furthermore, it was possible to obtain PVOH/cellulose microcomposites and PVOH/bentonite nanocomposites films, with good filler dispersion, by casting technique using water as solvent. Both fillers produced an increase in the glass transition temperature that can be mainly associated with the existence of filler–PVOH interactions, which was confirmed with FTIR measurements, and to a decrease the segmental motion of PVOH chain by the presence of filler. Additionally, a slight increase on the crystallinity of the microcomposites was registered only for higher contents of MC fibers; whereas the addition of bentonite caused a reduction on the crystalline phase in all cases. The incorporation of cellulose produced an increase on modulus but a clear decrease on tensile strength, which is related with the possible agglomeration of MC; whereas clay platelets were able to improve both, the tensile modulus and strength. Both fillers were also capable to reduce

the water absorption and the water vapor transmission rate of the neat matrix, being the effect higher in the case of cellulose. Although all the produced films were transparent, which is required for packaging, for high cellulose content this transparency was reduced.

Regarding PVOH/bentonite nanocomposites, independently of the processing steps, all the materials exhibited an intercalated–exfoliated mixed structure, as it was revealed from XRD patterns. In general terms, the best results were obtained in the case where the matrix and the clay were swelled together, which can also be related with the dispersion of the clay inside the matrix. On the other hand, the less significant changes were obtained for the sample NB, where the clay was not previously swelled.

All the obtained results seem to indicate that both materials could be used in a future for packaging applications but further studies should be carried out in order to confirm that.

Acknowledgements The authors would like to acknowledge the financial support of the National Research Council of Argentina (CONICET), National University of Mar del Plata (UNMdP), and the National Agency of Scientific and Technologic Promotion (ANPCyT), Fonarsec FSNano004.

References

1. Krumova M, Lopez D, Benavente R, Mijangos C, Perena JM (2000) Polymer 41:9265
2. Lopez D, Cendoya I, Torres F, Tejada J, Mijangos C (2001) J Appl Polym Sci 82:3215
3. Sinha RS, Bousmina M (2005) Prog Mater Sci 50:962
4. Kaczmarek H, Podgórski A (2007) J Photochem Photobiol A 191:209
5. Jang J, Lee DK (2003) Polymer 44:8139
6. Döppers LM, Breen C, Sammon C (2004) Vib Spectrosc 35:27
7. Pal K, Banthia K, Majumdar DH (2006) J Biomater Appl 21:75
8. Maria T, De Carvalho RA, Sobral PJ, Habitante AM, Solorza-Feria J (2008) J Food Eng 87:191
9. Peng Z, Kong LX, Li SD (2005) Polymer 46:1949
10. Sorrentino A, Gorrasi G, Vittoria V (2007) Trends Food Sci Technol 18:84
11. Qiu K, Netravali AN (2012) Compos Sci Technol 72:1588
12. Sriupayo J, Supaphol P (2005) Polymer 46:5637
13. García de Rodriguez NL, Thielmans W, Dufresne A (2006) Cellulose 13:261
14. Kvien I, Oskman K (2007) Appl Phys A Mater 87:641
15. Alexandre M, Dubois P (2000) Mater Sci Eng 28:1
16. Ray SS, Bousmina M (2006) In: Mai Y-W, Yu Z-Z (eds) Polymer nanocomposite. Woodhead Publishing, Cambridge, p 57
17. Silva SML, Araujo PER, Ferreira KM, Canedo EL, Carvalho LH, Raposo CMO (2009) Polym Eng Sci 49:1696
18. Choudalakis G, Gotsis AD (2009) Eur Polym J 45:967
19. Ludueña LN, Alvarez VA, Vazquez A (2007) Mat Sci Eng A Struct 460–461:121
20. Ollier R, Vázquez A, Alvarez V (2011) In: Bartul Z, Trenor J (eds) Advances in nanotechnology. Nova Publishers, New York, p 281
21. Casco M, Ludueña L, Vázquez A, Alvarez V (2010) In: Wythers M (ed) Advances in materials science research. Nova Publishers, New York, p 287
22. Ibrahim MM, El-Zawawy WK, Nassar MA (2010) Carbohydr Polym 79:694
23. Sharaf F, El-Eraki M, El-Gohary A, Ahmed F (1996) Polym Degrad Stab 47:343
24. Gupta S, Pramanick AK, Kailath A, Mishra T, Guha A, Nayar S, Sinha A (2009) Colloid Surf B 74:186
25. Razzak MT, Darwis D, Sukirno Z (2001) Radiat Phys Chem 62:107
26. Abd El-Kader KAM, Abdel Hamied SF, Mansour AB, El-Lawindy AM, El-Tantaway F (2002) Polym Test 21:847
27. Faruk O, Bledzkia AK, Fink HP, Sain M (2012) Prog Polym Sci 37:1552
28. Lu J, Wang T, Drzal LT (2008) Compos A Appl Sci 39:738
29. Roohani M, Habibi Y, Belgacem N, Ebrahim G, Karimi A, Dufresne A (2008) Eur Polym J 44:2489
30. Siracusa V, Rocculi P, Romani S, Dalla Rosa M (2008) Trends Food Sci Technol 19:634
31. Sanchez-Garcia MD, Gimenez E, Lagaron JM (2008) Carbohydr Polym 71:235
32. Gwon JG, Lee SY, Doh GH, Kim JH (2010) J Appl Polym Sci 116:3212
33. Fortunati E, Puglia D, Monti M, Santulli C, Maniruzzaman M, Kenny JM (2013) J Appl Polym Sci 128:3220
34. Dubief D, Samain E, Dufresne A (1999) Macromolecules 32: 5765
35. Samir M, Alloin F, Dufresne A (2005) Biomacromolecules 6:612
36. Gillman GP, Sumpter EA (1986) Aust J Soil Res 24:173
37. Majdzadeh-Ardakania K, Nazari B (2010) Compos Sci Technol 70:1557
38. Ali SS, Tang X, Alavi S, Faubion J (2011) J Agric Food Chem 59:12384
39. Farmer VC (1974) In: Farmer VC (ed) The infrared spectra of clay minerals. Mineralogical Society, London, p 331
40. Madejová J (2003) Vib Spectrosc 31:1
41. Lange J, Wyser Y (2003) Packag Technol Sci 16:149
42. Strawhecker KE, Manias E (2000) Chem Mater 12:2943
43. Sapalidis AA, Katsaros FK, Romanos GE, Kakizis NK, Kanellopoulos NK (2007) Compos B Eng 38:398
44. Leszczynska A, Njuguna J, Pielichowski K, Banerjee JR (2007) Thermochim Acta 454:1
45. Alkan M, Benlikaya R (2009) J Appl Polym Sci 112:3764
46. Chang JH, Jang TG, Ihn KJ, Lee WK, Sur GS (2003) J Appl Polym Sci 90:3208
47. Jia X, Li Y, Zhang B, Cheng Q, Zhang S (2008) Mater Res Bull 43:611
48. Lu C, Mai Y (2007) Compos Sci Technol 67:2895
49. Sapalidis AA, Katsaros FK, Steriotis TA, Kanellopoulos NK (2012) J Appl Polym Sci 123:1812